ARTICLE NO. 78-1692R

080
G80-

80006

Shaped Torque Techniques

C.J. Swigert*
Hughes Research Laboratories, Malibu, Calif.

Procedures are developed for synthesizing torque waveforms to optimally move a mechanical element of a structure so that the mechanical modes of oscillation of the structure are left unexcited at the end of the movement. A primary application of these procedures is in spacecraft missions that require reorientation of parts of the sparecraft without exciting resonant modes of the overall structure. The same procedures can synthesize driving force waveforms for translation of mechanical elements with mode suppression and can synthesize multiple torque and force waveforms with mode suppression in large complex structures. Constraints on the waveform synthesis procedure generally require that the resonant modes of the structure be excited during the torque period. At the end of the torque period, all of the resonant modes (and their derivatives) can be brought to zero amplitude. The torque synthesis procedure obtains the driver waveform that satisfies the boundary conditions on the structural modes. An analytic computer simulation is developed and exercised to obtain these shaped torque waveforms and the responses of the modes of selected structures. A hardware structure has been developed and exercised to evaluate the effects of error sources on this technique.

Introduction

RAPID repointing of a large controllable structure will generally excite many of the resonant modes of the structure. The vibrations of the modes in an optical or microwave structure will cause aberrations in the aperture wavefront and degradation in the aperture gain. These effects can be greatly reduced in the rapid repointing maneuver if the torqueing function(s) minimally excites the structural resonant modes. It is the primary objective of the shaped torque (ST) procedure to be able to synthesize torque waveforms to rotate the structure (or elements of the structure) through a specified angle θ in a given time T, leaving the optical structure shape in the original optical form at the end of period T. All higher order derivatives of motion in the structure are also to be zero at the end of period T. Hence, the large controllable structure will be motionless in its new pointing position at the end of the specified period T.

A secondary objective of the ST procedure is to synthesize torque waveforms that are relatively insensitive to variations in the plant parameters. Rocket thrusts or spacecraft reconfigurations will shift the parameters of the equations of motion. A candidate cost function for torque optimization that minimizes the sensitivity to plant parameter variation is discussed later.

Farrenkopf[1] has determined optimal open-loop maneuver profiles for a dynamically simple spacecraft maneuvering between two quiescent states. In the free end point problem, the structural deformation and its time derivative are unconstrained at maneuver's end. For the constrained end point problem, these variables are required to vanish, which necessarily degrades the cost function.

This optimal open-loop maneuver is sensitive to variations in model parameters. A 4% reduction in the actual bending mode frequency ω_{nom} yields a residual bending mode error of 5×10^{-3} for the benign case of $\omega_{nom}T_a=10$. A 4% reduction in ω_{nom} for the severe maneuver with $\omega_{nom}T_a=1$ yields a residual bending mode error of 5.0. A modal frequency shift of 4% has been experimentally observed in the ST hardware, together with the modal residual response and the corrected modal response. The ST experimental results are quite sensitive to the performance criterion being minimized, as demonstrated later in cases 3 and 4.

Presented as Paper 78-1692 at the AIAA Conference on Large Space Platforms: Future Needs and Capabilities, Los Angeles, Calif., Sept. 27-29, 1978; submitted Nov. 22, 1978; revision received Feb. 11, 1980.

Index category: Structural Dynamics.

*Member, Technical Staff, Exploratory Studies Department.

Shaped Torque Procedure

The shaped torque waveform $u(t)$ is chosen to satisfy the specified boundary conditions for the state variables θ, r_1, $r_2,\ldots,r_m$, illustrated in Fig. 1. Candidate state variables can be displacements or rotations of the structure at specified locations. Nominal initial conditions on the state variables are

$$\theta(0)=\theta_0 \qquad \dot{\theta}(0)=0$$
$$r_m(0)=0 \qquad \dot{r}_m(0)=0 \qquad (m=1,\ldots,M) \tag{1}$$

where $\dot{r}$ means dr/dt. These conditions are nominal because the ST procedure allows these initial conditions to be nonzero.

It is desired to find a torque waveform $u(t)$ that at the end of period T obtains terminal boundary conditions:

$$\theta(T)=\theta_1 \qquad \dot{\theta}(T)=0$$
$$r_m(T)=0 \qquad \dot{r}_m(T)=0 \qquad (m=1,\ldots,M) \tag{2}$$

Choosing the state variables r_m with respect to a structural internal reference system simplifies the process of specifying boundary conditions on the rotated structure. These terminal boundary conditions are nominal because the ST procedure allows these conditions to be nonzero, e.g., $\dot{\Theta}(T)=\dot{\Theta}_1$ for constant slew rate.

In addition to boundary conditions, the ST procedure requires the structural dynamics to be characterized, e.g., by a

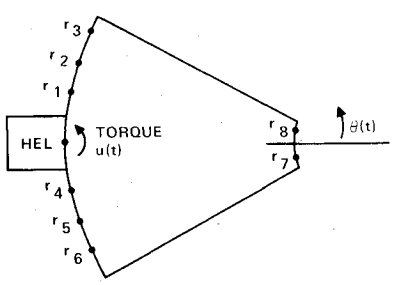

Fig. 1 State variables $\theta(t)$, $V_m(t)$, and torque function $u(t)$ for a large controllable structure.

set of differential equations that describe the response of the state variables to the torque forcing function $u(t)$. Controllability is assumed for the structure, in the classical sense,[2] i.e., that there is a $u(t)$, $0 \le t \le T$, that can satisfy the boundary conditions. There are other procedures for describing the dynamics of the large structure, such as in an energy formulation for wave motion in the structure, from which the equations of motion of the structure can be obtained. This set of differential equations, which are the structural equations of motion, are diagonalized into a new set of basis vectors, i.e., eigenvectors, that describe the modes of the structure. This diagonalization provides a one-to-one mapping between the $M+1$ state variables and the $M+1$ eigenvectors which characterize the modes of the system. The boundary conditions on the $M+1$ state variables map directly to a unique set of boundary conditions on the $M+1$ eigenvectors $y_m(t)$, $m=1,2,\ldots,M+1$, at time $t=0$ and $t=T$. What is of even more interest is that with linear constraints on the damping, the diagonalized set of eigenvectors have equations of motion of the form

$$\ddot{y}_m + d_m \dot{y}_m + \nu_m^2 y_m = c_m u(t) \qquad (m=1,2,\ldots,M+1) \quad (3)$$

All the mode boundary conditions can be satisfied with a torque function of the form

$$u(t) = \sum_{n=1}^{M+1} \exp(-\sigma_n t) \cdot [g_{1,n} \cos(\omega_n t) + g_{2,n} \sin(\omega_n t)] \quad (4)$$

for which arbitrarily preselected driving frequencies ω_n and damping σ_n can be selected. The following plausibility argument shows that $M+1$ is the correct number of terms for $u(t)$ in Eq. (4). The $M+1$ eigenvectors satisfy the initial boundary conditions, independent of $u(t)$. There are $2(M+1)$ boundary conditions on $y_m(T)$ and $\dot{y}_m(T)$ that must be obtained by $u(t)$. Hence, there are $2(M+1)$ constraints on $u(t)$. In Eq. (4), $u(t)$ has $2(M+1)$ degrees of freedom provided by $\{g_{1,n}, g_{2,n}\}$, $n=1,\ldots,M+1$. Since there are as many degrees of freedom as there are constraints, a $u(t)$ can be found that satisfies all the mode boundary conditions. In the following paragraphs, several examples will illustrate the form of $u(t)$.

Shaped Torque Evaluation

A computer simulation of the ST procedure has been developed that obtains $u(t)$, given the $M+1$ equations of motion of the modes and their boundary conditions, with $M \le 100$. Ultimately, the maximum size of M will probably be determined by the size of the numerical error that can be tolerated in the solution for $u(t)$. An experimental demonstration of the ST procedure has been developed that uses the $u(t)$ solution calculated by the computer simulation. The experimental testbed results are described in the concluding section.

It should also be noted that there is a continuum of solutions $u(t)$ in Eq. (4) that satisfies the boundary conditions since we are free to choose $\{\sigma_n, \omega_n\}$. There are a number of criteria that can be chosen to select an optimal torque waveform. One candidate performance index that will tend to minimize $u(t)$ over the entire interval $[0,T]$ is

$$J_1 = \int_0^T u(t)^2 dt \quad (5)$$

If $u(t)$ is chosent to minimize J_1, $u(t)$ will tend to be small over the full torque period. Applying the maximum principle[3] to minimize J_1, values for σ_m, ω_m are

$$\sigma_m = d_m/2 \qquad \omega_m = [\nu_m - (d_m/2)^2]^{1/2}$$

$$(m=1,2,\ldots M+1) \quad (6)$$

where d_m, ν_m, c_m are defined in Eq. (3). Parameters $g_{1,n}$ and $g_{2,n}$ in Eq. (4) are chosen to satisfy the boundary conditions in Eqs. (1) and (2).

Equation (4) illustrates a continuum of torque solutions $u(t)$ that can satisfy the boundary conditions in Eqs. (1) and (2). Minimizing a cost function such as J_1 yields a single torque function $u(t)$. For several applications of interest, this $u(t)$ is a poor solution. The modal responses are very sensitive to the modal resonance frequencies, i.e., the eigenfrequencies. If the resonances shift, e.g., due to mass expulsion or spacecraft reconfiguration, the modes' responses will change drastically. This is because the optimal torque function was operating on the peaks of the modal resonances. With a shift in frequency of the peaks, the torque function will be operating on the slopes of the modes' transfer functions.

Another candidate performance index J_2 reflects the concern for the accuracy of the terminal boundary conditions with changes in modal parameters. Ideally, the mode amplitudes $y_m(t=T)$ at the end of the maneuver should be unaffected by small changes in each of the mode eigenfrequencies. Hence, the choice of

$$J_2 = \sum_{m=1}^{M+1} \left(\frac{\partial y_m(t=T)}{\partial \nu_m} \right)^2 \quad (7)$$

Torque waveforms $u(t)$ that minimize J_2 are less sensitive to errors in the actual $u(t)$ or the plant parameter estimates. J_2 can be minimized by iteratively evaluating J_2 in the computer simulation for different positions of the poles of $u(t)$ in the s-plane. This iterative technique has been used to minimize J_1 numerically to converge to the analytic solution of J_1 given by Eq. (6).

The computer simulation has also been modified to allow numerical evaluation of the derivatives $\partial y_m / \partial \nu_m$ for a given $u(t)$. With small perturbations in ν_m, the preferred $u(t)$ to minimize J_2 can be determined. Two torque waveforms will be described in the following section; one of which minimizes J_1 but causes J_2 to be infinite. The second waveform has about double the value of the minimum J_1, but makes J_2 nearly zero.

Computer Simulation Results

A computer simulation of the ST procedure has been developed to obtain the torque function $u(t)$ and to evaluate the controlled state variables $\theta(t)$, $r_m(t)$, $m=1,\ldots,M$, and their derivatives $\dot{\theta}(t)$ and $\dot{r}_m(t)$, $m=1,\ldots,M$, over the time interval $t=0-2T$. The computer simulation also evaluates the response over the interval $[0, 2T]$ of uncontrolled state variables $r_m(t)$ and $\dot{r}_m(t)$, $m=M+1,\ldots 2M+2$, whose boundary conditions are not specified. The performance index J_1 in Eq. (5) is evaluated.

Table 1 illustrates several representative computer experiments to evaluate ST performance. Cases 1 and 2 with different torque functions illustrate rotation of the structure, i.e., eigenvector θ, a rigid-body mode, with one mode being controlled. The uncontrolled mode has r_1 and $\dot{r}_1$ both nonzero at $T=1$ s and continues to oscillate after $t=T$. Case 1 illustrates the optimum torque function for criterion J_1 with only the pointing mode being controlled. Figures 2 and 3 illustrate cases 1 and 2.

Cases 3 and 4 in Table 1 use different torque waveforms to rotate the rigid-body mode θ with the previously observed mode r_1 now being controlled. The two cases illustrate that there are many torque functions $u(t)$ that satisfy the boundary conditions, as noted in the preceding discussion of Eq. (4). The uncontrolled modes r_2 and r_3 are monitored. Note that r_2 and r_3 are both nonzero at $T=1$ s and continue to oscillate after $t=T$. Case 3 illustrates the optimum torque function for criterion J_1 with the additional mode being controlled.

Table 1 Shaped torque cases for $\theta(T)=0.025$ rad, $T=1$ s

Case	Controlled modes	Uncontrolled modes observed	Torque features	$J_1=\int u^2 dt$
1	$\ddot{\theta}=u(t)$	$\ddot{r}_1+400r_1=100u(t)$	Ramp	0.0075
2	Same as 1	Same as 1	Bang-bang	0.0100
3	$\ddot{\theta}=u(t)$ $\ddot{r}_1+400r_1=100u$	$\ddot{r}_2+484r_2=100u(t)$ $\ddot{r}_3+576r_3=100u(t)$	Ramp + term with $\omega_1=20$ rad/s	0.0084
4	Same as 3	Same as 3	$\omega_1=\pi$ rad/s $\omega_2=3\pi$ rad/s	0.0150
5	$\ddot{\theta}=u(t)$ $\ddot{r}_1+400r_1=100u(t)$ $\ddot{r}_2+484r_2=100u(t)$ $\ddot{r}_3+576r_3=100u(t)$		Ramp + terms with $\omega_1=20.0$ rad/s $\omega_2=22.0$ rad/s $\omega_3=24.0$ rad/s	0.0092

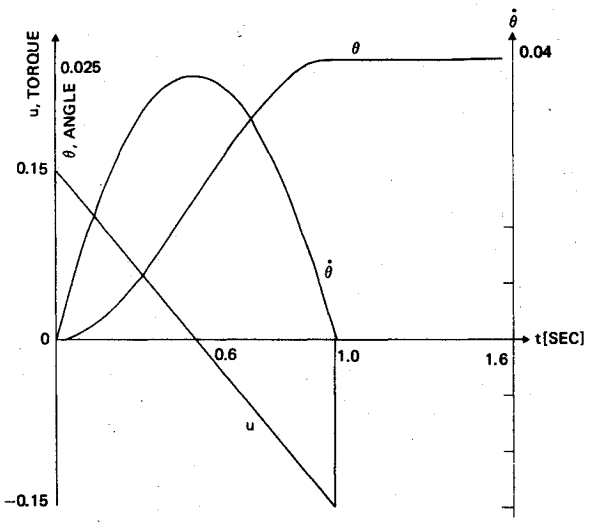

Fig. 2a Ramp torque control for rigid-body θ, case 1.

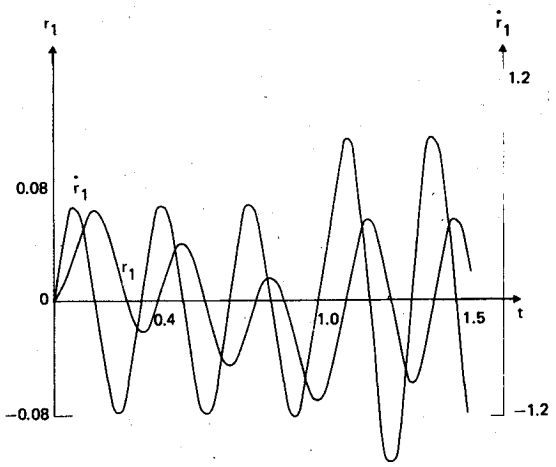

Fig. 2b Ramp torque waveform drives r_1 in case 1, $\ddot{r}_1+400\,r_1=100\,u$.

Case 4 illustrates a $u(t)$ with minimum change in terminal boundary with change in modal resonance, though J_1 is almost doubled. Case 3 minimizes J_1 and not J_2 with

$$\left.\frac{\partial\theta(t=1)}{\partial v_0}\right|_{v_0=0}=-\infty \qquad \left.\frac{\partial r_1(t=1)}{\partial v_1}\right|_{v_1=20}=1.08 \tag{8a}$$

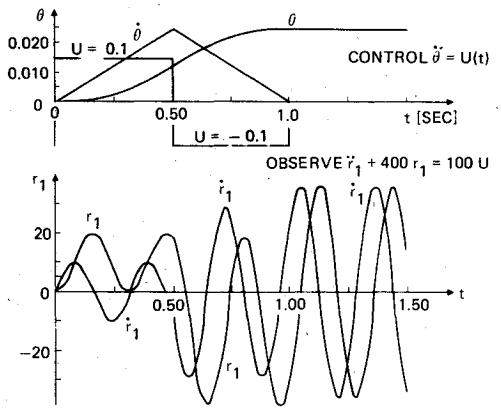

Fig. 3 Bang-bang torque control of θ with mode r_1 observed, case 2.

to give

$$J_2=\infty \tag{8b}$$

For Case 4, which attempts to minimize J_2,

$$\left.\frac{\partial\theta(t=1)}{\partial\varphi_0}\right|_{v_0=0}=0 \qquad \left.\frac{\partial r_1(t=1)}{\partial v_1}\right|_{v_1=20}=1.27\times10^{-3} \tag{9a}$$

for

$$J_2=1.6\times10^{-6} \tag{9b}$$

Hence, if there is more concern about the accuracy of the terminal boundary conditions, $u(t)$ for case 4 is much preferred to that for case 3. Figures 4 and 5 illustrate cases 3 and 4, respectively. Modes r_3 and $r_4(t)$ in Fig. 5 illustrate the small change in response with change in modal resonance due to $u(t)$ in case 4. Compare modes r_3 and $r_4(t)$ in Fig. 5 with Fig. 4 for $u(t)$ that minimizes J_1, but not J_2.

Case 5 in Table 1 illustrates rotation of the structure θ with the additional modes r_2 and r_3 being controlled. Note that all modes achieve their boundary conditions at $T=1$ s with all higher order time derivatives zero thereafter. The structrure in case 5 is motionless after the end of this torque period. Figure 6 illustrates case 5.

Experimental Demonstration

An experimental demonstration of the ST procedure has been developed to aid the error analysis and assessment for boundary condition control. A generalized ST testbed

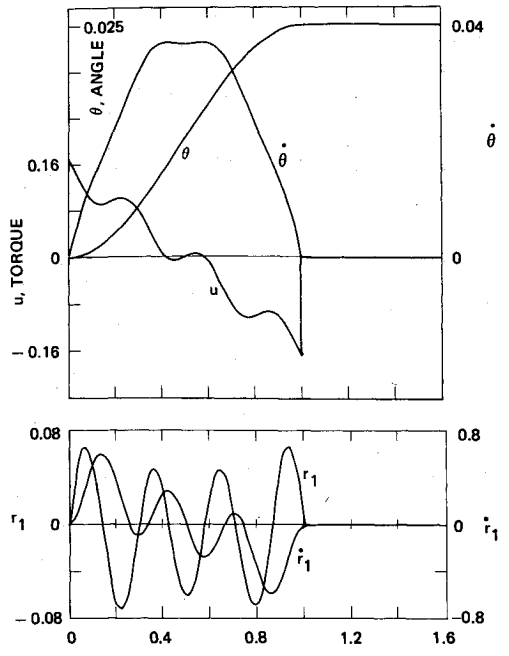

Fig. 4a Minimum least-squares torque waveform controls θ and r_1 in case 3.

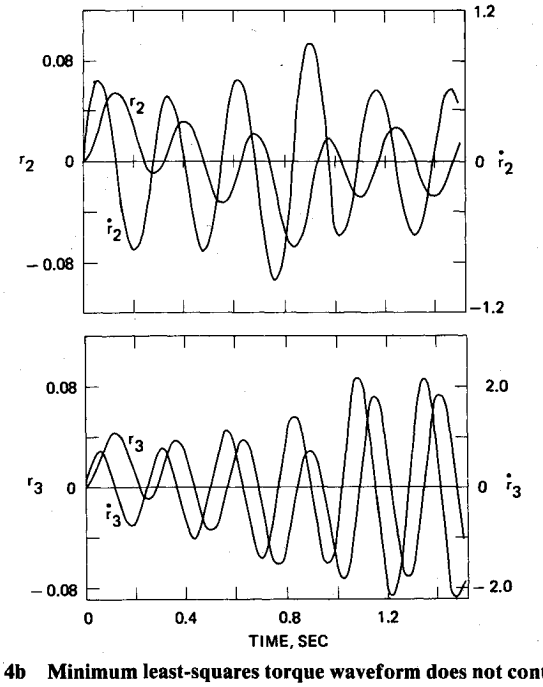

Fig. 4b Minimum least-squares torque waveform does not control r_2 and r_3 in case 3. Compare response with Fig. 5b.

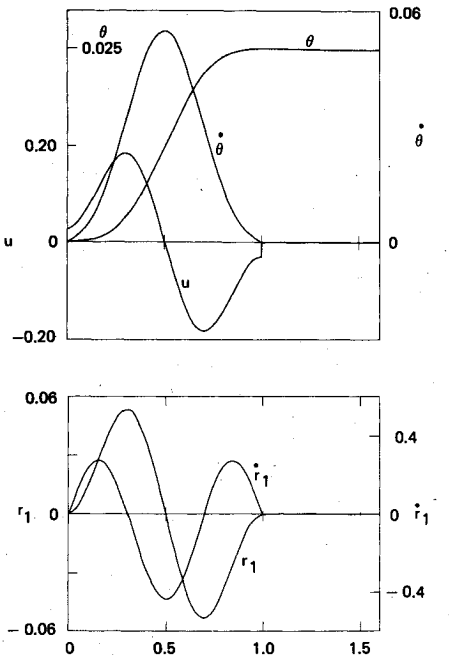

Fig. 5a Torque for minimal response variation controls θ and r_1 in case 4.

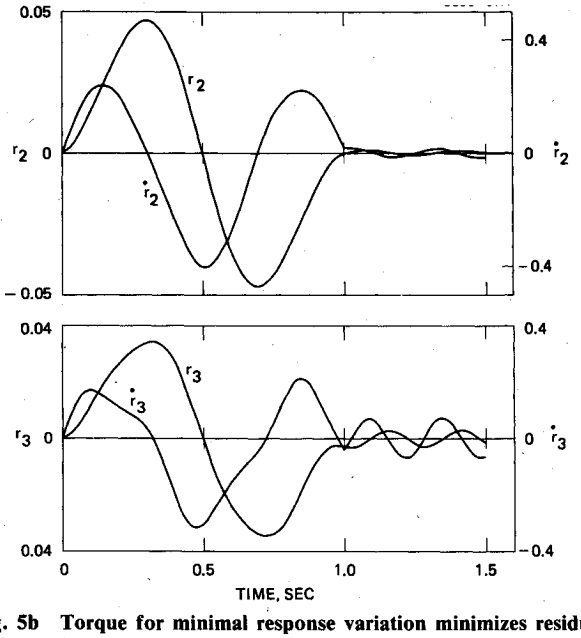

Fig. 5b Torque for minimal response variation minimizes residual response ($t>1$ s) for modes r_2 and r_3 in case 4. Compare response with Fig. 6b.

structure has been built which can be set up with a specified number of modes (Fig. 7). A permanent-magnet dc motor with a rotor flywheel introduces the ST to the structure. The dc motor is controlled by a microcomputer which generates the ST waveform. Figure 8 illustrates the signal flow in the ST testbed.

Construction of the ST waveform is a two-step process. The first step is parameter identification of the structural modes. The second step is to use the modal equations of motion to obtain the ST waveform from the analytic computer simulation.

Figure 9 illustrates a five-mass model of the ST testbed configuration and the five modes. Mode e_0 is the rigid-body mode. Modes e_1 and e_2 are asymmetric, resonant modes excited by the centrally placed torque motor. Modes e_3 and e_4 are symmetric modes and not excited by the centrally placed torque motor. The mode equations of motion are

$$\ddot{y}_0 = c_0 u \tag{10a}$$

$$\ddot{y}_1 + \omega_1^2 y_1 = c_1 u \tag{10b}$$

$$\ddot{y}_2 + \omega_2^2 y_2 = c_2 u \tag{10c}$$

where y_i is the temporal response of mode e_i at a specific point, namely M_3. Modes y_3 and y_4 are not excited or controllable by $u(t)$ because the testbed is symmetric about the torque driving point.

The ST problem of controlling mode responses y_0 and y_1 and observing y_2 will be treated. The terminal boundary

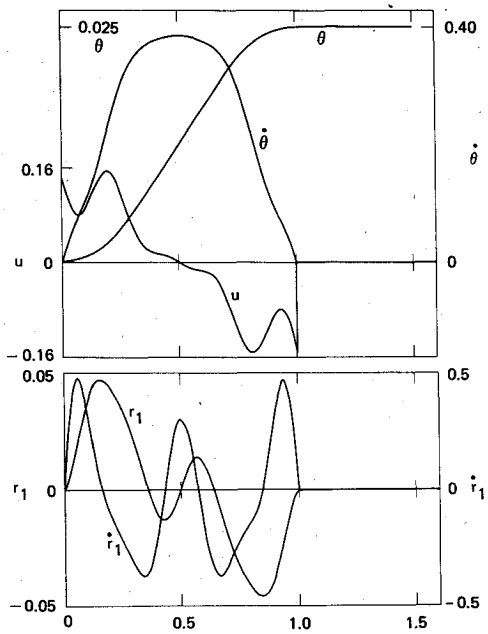

Fig. 6a Minimum least-squares torque waveform $u(t)$ controls four modes: θ, r_1.

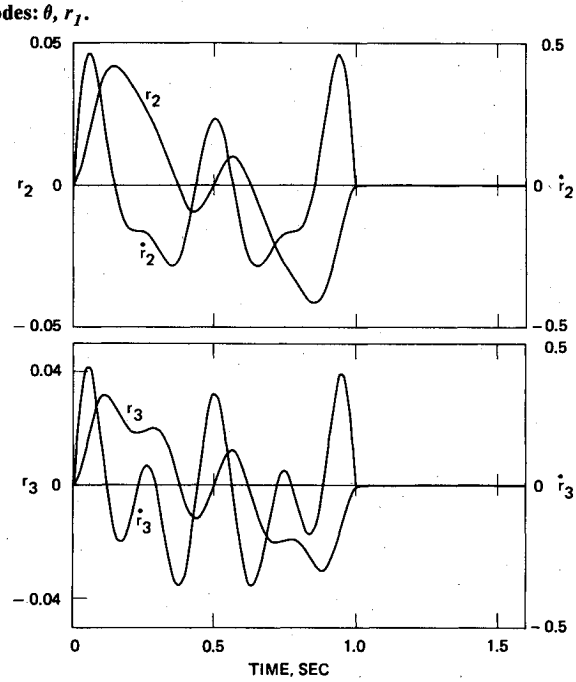

Fig. 6b Minimum least-squares torque waveform $u(t)$ controls four modes: r_2, r_3.

conditions on y_0 and y_1 are

$$y_0(T)=y \qquad y_1(T)=0$$
$$\dot{y}_0(T)=0 \qquad \dot{y}_1(T)=0 \tag{11}$$

A frequency analysis was employed for parametric estimation of c_0, c_1, c_2 and ω_1, ω_2. Twin accelerometers are mounted at each M_3 position in Fig. 9. Voltage V_s drives the motor servo. Accelerometer output voltage V_a is measured. The Laplace transfer function can be shown to be

$$G(s)=\frac{V_a(s)}{V_s(s)}=\frac{Ks(s^2-\omega_0^2)}{s^2+\delta s+\omega_1^2} \tag{12}$$

$G(s)$ parameters K, ω_0, ω_1, and δ are related to the structural parameters, including I_1, M_2, and M_3, distance R_i between lumped parameters, and a small damping D due to pivot friction.

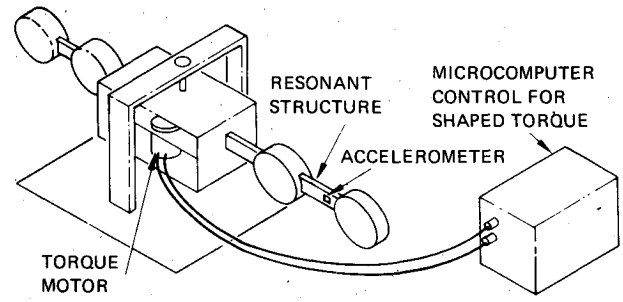

Fig. 7 Shaped torque testbed structure.

The frequency analysis measured $G(s)$ at different frequencies, using the microcomputer output V_s to drive the structure with sinusoidal $u(t)$. The microcomputer is also able to record the sinusoidal accelerometer output

$$V_a=K_{\text{accel}}\ddot{x}_a=RK_{\text{accel}}\ddot{\theta}_a \tag{13}$$

and the drive motor tachometer output

$$V_{\text{tach}}=K_{E_g}\dot{\theta}_m \tag{14}$$

From V_{tach} we can obtain the torque applied by the rotor

$$T=I_{\text{rotor}}\ddot{\theta}_m \tag{15}$$

Figure 10 illustrates the measured transfer function and the curve fit to the data, namely

$$G(f)=\frac{0.00653f(f^2+10.2^2)}{(9.64^2-f^2)+j\,0.095f} \tag{16}$$

Ignoring the damping, the estimated parameters of the structures yield the mode equations

$$6.45\times10^{-7}\ u=\ddot{y}_0 \tag{17a}$$
$$9.96\times10^{-6}\ u=\ddot{y}_1+3.59\times10^3 y_1 \tag{17b}$$
$$5.33\times10^{-6}\ u=\ddot{y}_2+3.54\times10^5 y_2 \tag{17c}$$

Figure 11 illustrates the actual accelerometer response to a bang-bang torque waveform with period $T=0.1032$ s to strongly excite the 9.6-Hz resonant mode. Note the strong response of the mode to this torque waveform chosen to rotate the structure through 25 mrad. The oscilloscope trace shows both the structural response at the accelerometer and the motor velocity $\dot{\theta}_m$ measured by the tachometer.

Figure 12 illustrates the ST waveform analogous in Table 1 to case 4 with minimum J_2 cost function. The waveform is chosen to rotate the structure through 25 mrad with period $T=0.1032$ s, as for the preceding bang-bang case. We have ST waveform and motor velocity

$$u(t)=9.66\cos\omega_1 t+17.3\cos\omega_2 t \qquad (0<t<T) \tag{18a}$$
$$\dot{\theta}_m(t)=63.5\sin w_1 t+37.9\sin w_2 t \tag{18b}$$

Both $u(t)$, $\dot{\theta}_m(t)$ and the theoretical response of the 9.6-Hz mode are shown in Fig. 12.

Figure 13 illustrates the actual accelerometer response and motor velocity for the ST waveform in Eqs. (18). The response of the 9.6-Hz mode is nonzero, but small at the end of the torque period. The 9.6-Hz mode response is seen better in Fig. 14 with the digital filter (Fig. 8) removing the 90-Hz mode response. Filter corner frequencies are at 2.2 and 22Hz. The 9.6-Hz mode response is 1/6 of the bang-bang waveform response.

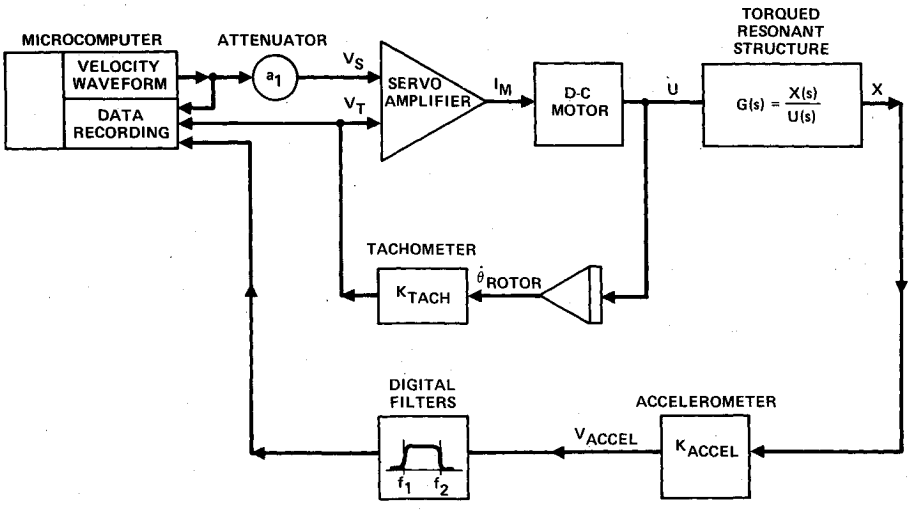

Fig. 8 Signal flow in shaped torque testbed experiment.

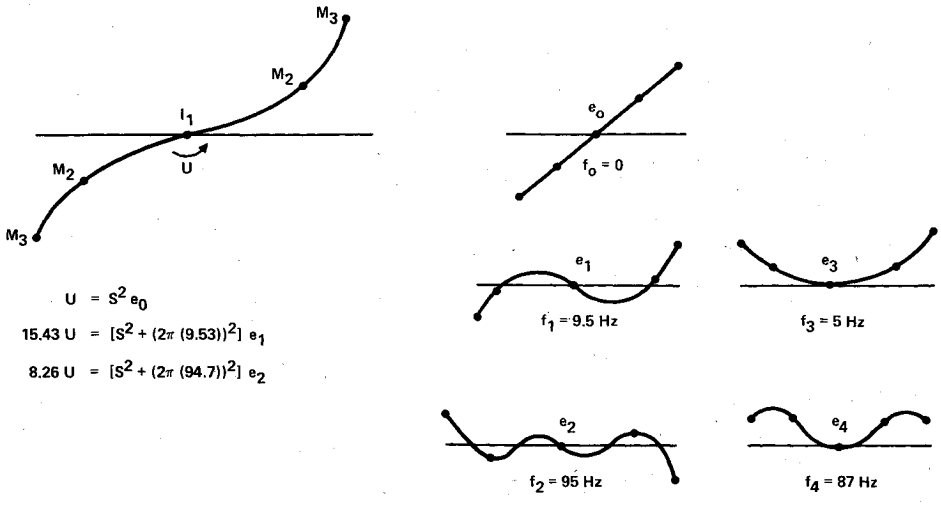

$$U = S^2 e_0$$

$$15.43\,U = [S^2 + (2\pi\,(9.53))^2]\,e_1$$

$$8.26\,U = [S^2 + (2\pi\,(94.7))^2]\,e_2$$

Fig. 9 Shaped torque testbed model and five modes.

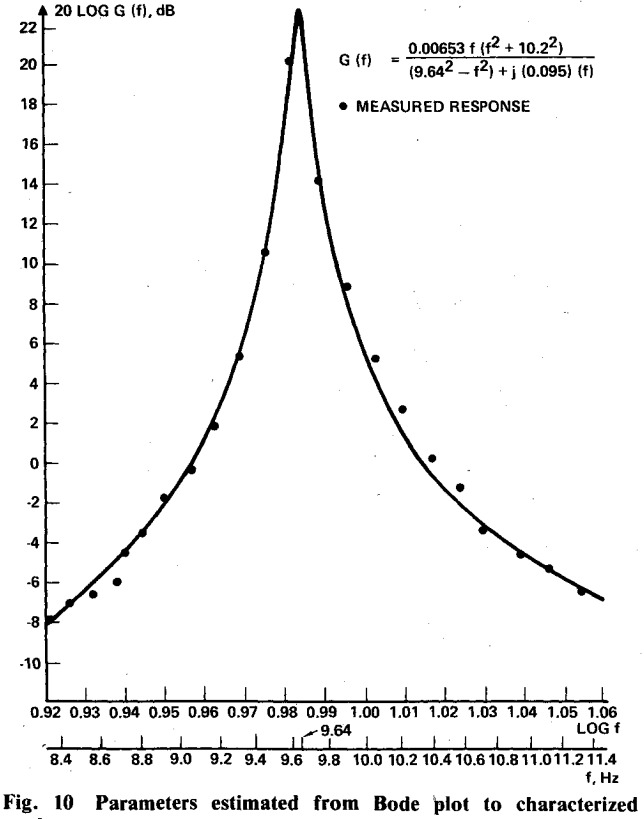

Fig. 10 Parameters estimated from Bode plot to characterized mode e_1.

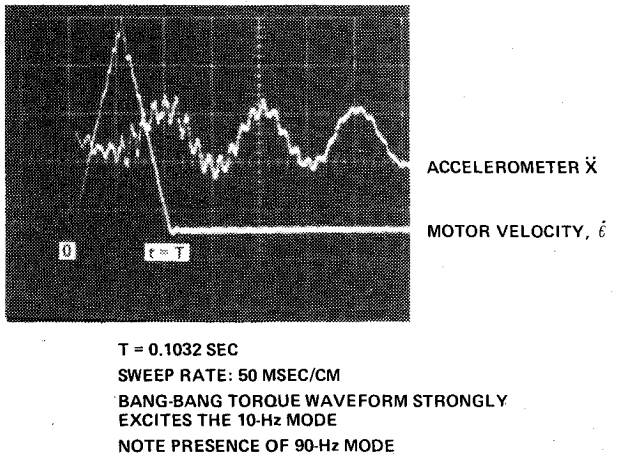

Fig. 11 Bang-bang torque waveform and accelerometer response.

Figure 15 illustrates reduction of the 9.6-Hz mode response by 50% with a modified torque motor velocity.

$$\dot{\theta}_m(t) = 63.5\,\sin\omega_1 t + 34.\,\sin\omega_2 t \qquad (0 < t < T) \tag{19}$$

The 9.6-Hz mode response is 1/12 of the bang-bang response.

Figure 16 illustrates no discernible response of the 9.6-Hz mode with the improved torque motor velocity.

$$\dot{\theta}_m(t) = 63.5\,\sin\omega_1 t + 30.\,\sin\omega_2 t \qquad (0 < t < T) \tag{20}$$

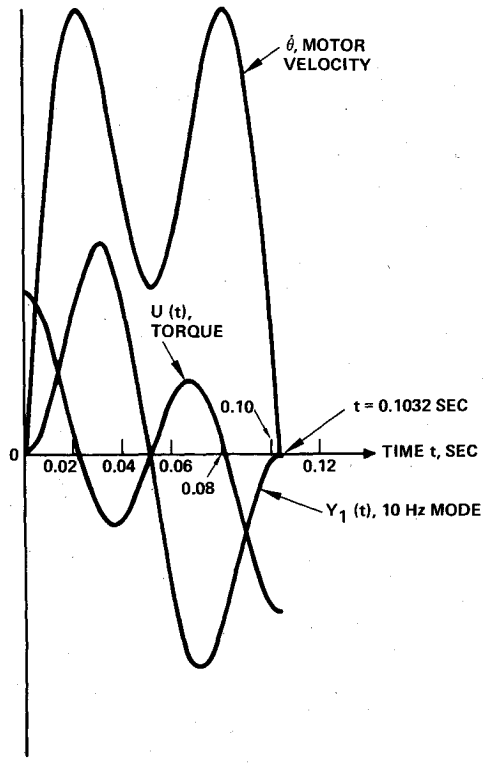

Fig. 12 Theoretical ST waveform chosen for experimental control of modes e_0 and e_1.

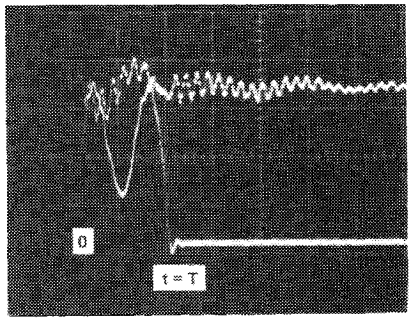

T = 0.1032 SEC
SWEEP RATE: 50 MSEC/CM
SHAPED TORQUE WAVEFORM DERIVED BY PARAMETER ESTIMATION, SCALED TO ROTATE TESTBED SAME AS BANG-BANG WAVEFORM
DESIGNED TO CONTROL 10-Hz MODE TO ZERO
10-Hz MODE RESPONSE IS 1/6 OF BANG-BANG RESPONSE (17%)
$U(t) = 9.66 \cos \omega_1 t + 17.3 \cos \omega_2 t \quad 0 < t < T$
$\dot{\theta}(t) = 63.5 \sin \omega_1 t + 37.9 \sin \omega_2 t$

Fig. 13 ST waveform in Fig. 12 and accelerometer response.

Removing the digital filtering of the 90-Hz mode, Figure 17 illustrates the actual accelerometer response. The response of the 90-Hz mode can also be suppressed by extending the ST waveform to control that mode as well.

This demonstration of adaptive correction of the control law on the testbed shows that the effects of model errors can be eliminated by iteration. An error analysis shows that for Eq. (20) to be correct, the originally measured 9.6-Hz mode must have shifted to a new resonant frequency of 10.06 Hz. This new resonant frequency was verified experimentally and seen to be due to the method of attachment of the flexible arms to the testbed body.

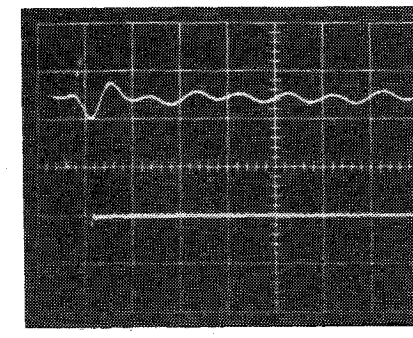

T = 0.1032 SEC
SWEEP RATE: 100 MSEC/CM.
$\dot{\theta}(t) = 63.5 \sin \omega_1 t + 37.9 \sin \omega_2 t \quad 0 < t < T$
RESPONSE IS BANDPASS FILTERED
CORNER FREQUENCIES AT 2.2 Hz, 22 Hz
PEAK-PEAK DEFLECTION OF 10-Hz MODE ≈ 0.2 CM
10-Hz MODE RESPONSE IS 1/6 OF BANG-BANG (-16 dB)

Fig. 14 ST waveform in Fig. 12 and filtered accelerometer response.

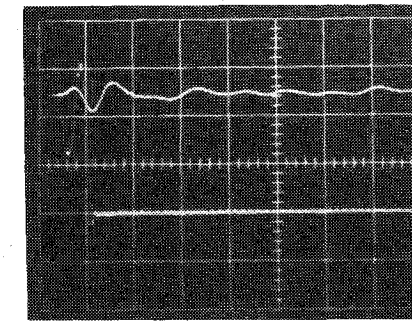

T = 0.1032 SEC
SWEEP RATE: 100 MSEC/CM
$\dot{\theta}(t) = 63.5 \sin \omega_1 t + 34 \sin \omega_2 t$
RESPONSE BANDPASS FILTERED (2.2 Hz, 22 Hz)
PEAK-PEAK DEFLECTION OF 10-Hz MODE ≈ 0.1 CM
10-Hz MODE RESPONSE IS 1/12 OF BANG-BANG (-22 dB)

Fig. 15 Modified ST waveform from Fig. 14 and filtered accelerometer response.

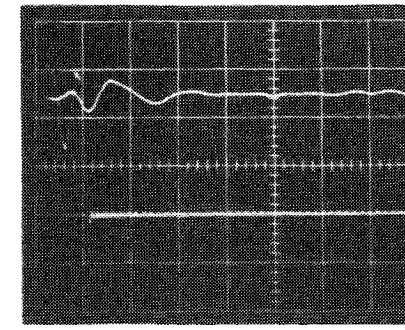

T = 0.1032 SEC
SWEEP RATE: 100 MSEC/CM
$\dot{\theta}(t) = 63.5 \sin \omega_1 t + 30 \sin \omega_2 t$
RESPONSE BANDPASS FILTERED (2.2 Hz, 22 Hz)
NO DISCERNIBLE RESPONSE OF 10-Hz MODE

Fig. 16 Modified ST waveform from Fig. 15 and filtered accelerometer response.

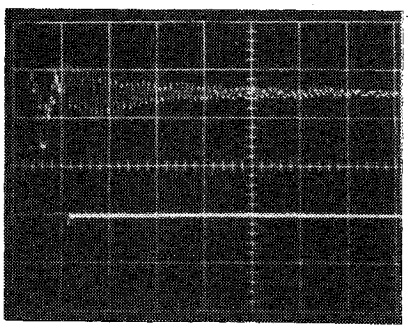

Fig. 17 Modified ST waveform from Fig. 15 and filtered accelerometer response.

Conclusion

The shaped torque technique for control of terminal boundary conditions has been evaluated in an analytic computer simulation and in a hardware testbed structure. A secondary objective has been to synthesize torque waveforms that are relatively insensitive to varitions in the plant parameters. We have demonstrated that torque waveforms optimized for minimum torque, i.e., for minimum J_1, are very sensitive to parameter variation. Torque waveforms have been domonstrated that are insensitive to plant variations, i.e., minimize J_2. We have also demonstrated adaptive correction of the control law on the testbed in the presence of additional modes to show that the effects of model errors can be eliminated by iteration.

References

[1] Farrenkopf, R.L., "Optimal Open-Loop Maneuver Profiles," AIAA Paper 78-1280, AIAA Guidance and Control Conference, Aug. 1978.

[2] Zadeh, L.A., and Desoer, C.A., *Linear System Theory: The State Space Approach*, McGraw-Hill, New York, 1963, p. 498.

[3] Sage, A.P., *Optimum Systems Control*, Prentice Hall, Englewood Cliffs, N.J., 1968, p. 57.